

FIDUCIAL STELLAR POPULATION SEQUENCES FOR THE VJK_S PHOTOMETRIC SYSTEMCRYSTAL M. BRASSEUR¹, PETER B. STETSON², DON A. VANDENBERG¹, LUCA CASAGRANDE³, GIUSEPPE BONO⁴, MASSIMO DALL'ORA⁵¹Department of Physics & Astronomy, University of Victoria, P.O. Box 3055, Victoria, B.C., V8W 3P6, Canada²Herzberg Institute of Astrophysics, National Research Council Canada, 5071 W. Saanich Rd., Victoria, B.C., V9E 2E7, Canada³Max-Planck-Institut für Astrophysik, Postfach 1317, 85748 Garching, Germany⁴Universita' di Roma Tor Vergata, Via della Ricerca Scientifica 1, 00133 Rome, Italy⁵INAF-Osservatorio Astronomico di Capodimonte, Via Moiariello 16, 80131 Napoli, Italy

THE ASTRONOMICAL JOURNAL, ACCEPTED

ABSTRACT

We have obtained broad-band near-infrared photometry for seven Galactic star clusters (M92, M15, M13, M5, NGC 1851, M71 and NGC 6791) using the WIRCam wide-field imager on the Canada-France-Hawaii Telescope, supplemented by images of NGC 1851 taken with HAWK-I on the VLT. In addition, 2MASS observations of the $[\text{Fe}/\text{H}] \approx 0.0$ open cluster M67 were added to the cluster database. From the resultant $(V-J)-V$ and $(V-K_S)-V$ colour-magnitude diagrams (CMDs), fiducial sequences spanning the range in metallicity, $-2.4 \lesssim [\text{Fe}/\text{H}] \lesssim +0.3$, have been defined which extend (for most clusters) from the tip of the red-giant branch (RGB) to ~ 2.5 magnitudes below the main-sequence turnoff. These fiducials provide a valuable set of empirical isochrones for the interpretation of stellar population data in the 2MASS system. We also compare our newly derived CMDs to Victoria isochrones that have been transformed to the observed plane using recent empirical and theoretical colour- T_{eff} relations. The models are able to reproduce the entire CMDs of clusters more metal rich than $[\text{Fe}/\text{H}] \approx -1.4$ quite well, on the assumption of the same reddenings and distance moduli that yield good fits of the same isochrones to Johnson-Cousins $BV(RI)_C$ photometry. However, the predicted giant branches become systematically redder than the observed RGBs as the cluster metallicity decreases. Possible explanations for these discrepancies are discussed.

1. INTRODUCTION

The Two Micron All Sky Survey (2MASS) has uniformly scanned the entire sky in three near-infrared bands, JHK_S . Cataloging more than 300 million point sources, 2MASS observations are not only advancing our understanding of stars, but they also provide the photometric standards used to calibrate all other JHK_S photometry. In recent years, a new generation of JHK_S equipped observing facilities have come online, driven by the benefits of observing at these longer wavelengths. In particular, reduced dust attenuation allows the near-infrared to be a better probe of stellar populations in dust-obscured and heavily reddened galaxies. Furthermore, the integrated luminosities of intermediate-age and old stellar populations, which are predominantly due to their asymptotic-giant-branch (AGB) and red-giant-branch (RGB) stars, are brightest at these longer wavelengths.

As the infrared (IR) region of the electromagnetic spectrum receives growing attention in modern astrophysics, it becomes desirable to have deep near-IR photometry for Galactic star clusters. Currently, the available near-IR fiducials of these systems remain restricted in both metallicity and luminosity, with the observations rarely extending to fainter magnitudes than the base of the RGB (e.g., Frogel et al. 1983; Valenti, Ferraro, & Origlia 2007; Ferraro et al. 2000). Star clusters are the ideal stellar populations to observe because, notwithstanding a growing number of exceptions (e.g., ω Cen), their stars are or can be considered homogeneous in both age and initial chemical composition to a rather good approximation, at least for a number of purposes. Therefore, observations of these systems provide us with exceedingly valuable stellar population templates across a broad range of stellar parameter space, as well as the data which are needed to test and refine the predicted colours from model atmospheres and the temperatures

given by stellar evolutionary models.

Stellar population studies rely on the accuracy of both colour- T_{eff} relations and the stellar T_{eff} scale in order to derive the ages, metallicities, and star formation histories of stellar systems based on isochrone fits to observed colour-magnitude diagrams (CMDs). One way to test these relations is to obtain photometry in many bandpasses and then to determine the level of consistency across all possible CMDs (and colour-colour diagrams) that can be generated. While considerable work has been carried out to test and improve the colour transformations for the $BV(RI)_C$ and Strömgren filter systems (e.g., Vandenberg & Clem 2003; Clem et al. 2004), very little has been done to date on the colour- T_{eff} relations for the near-IR (two of the few works to date are Pinsonneault et al. (2004) and citetGS2003).

In this paper, new CMDs for open and globular star clusters, along with published data for field subdwarfs, are compared with isochrones in order to assess the reliability of recent $(V-J)-T_{\text{eff}}$ and $(V-K_S)-T_{\text{eff}}$ relations. Additionally, and perhaps most importantly, we can for the first time evaluate the consistency of the isochrone fits across optical and infrared colours. The companion work to this paper, Vandenberg et al. (AJ, submitted); hereafter known as VCS10), focusses on the colour- T_{eff} relations for the Johnson-Cousins $BV(RI)_C$ photometric system. In both papers, two recently developed sets of colour transformations are tested. The first of these has been derived (see VCS10) from the latest MARCS model atmospheres (Gustafsson et al. 2008), while the second is the set of empirical relations developed by Casagrande et al. (2010) who used the Infrared Flux Method (IRFM) to produce colour- T_{eff} relations for dwarf and subgiant stars spanning a large range in metallicity.

Addressing the need for precise fiducial sequences in the near-infrared, we have obtained observations of the seven Galactic star clusters, M92, M15, M13, M5, NGC1851, M71 and NGC6791. In §2, we describe our observing programs and present salient details concerning the reduction of the data — including, in particular, the calibration of our photometry to the standard 2MASS system. In §2.1, the CMDs and cluster fiducials are presented which provide template stellar population sequences for the range in metallicity, $-2.4 \lesssim [\text{Fe}/\text{H}] \lesssim +0.3$. An examination of how well isochrones that employ the synthetic MARCS, and the empirical Casagrande et al. (2010), colour- T_{eff} relations are able to reproduce the observed VJK_S photometry of the local subdwarfs and of our target clusters is presented in §3. Finally, a short summary of our results, as well as a brief discussion of the usefulness of the derived fiducial sequences for stellar populations research, is given in §4.

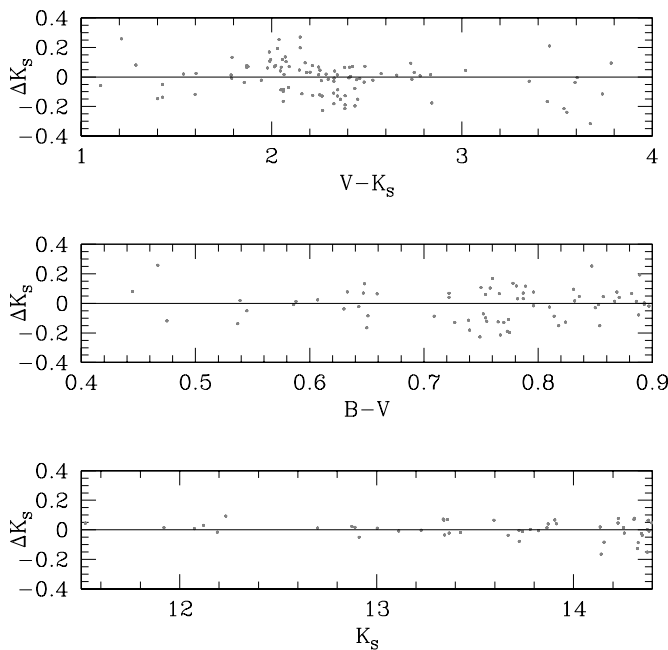


FIG. 1.— K_S -band photometric differences for stars observed in both 2MASS and our VLT fields for NGC 1851.

2. OBSERVATIONS

In the 2008B semester, we received WIRC*am* time on the CFHT to observe five Galactic star clusters (NGC6791, M13, M15, M92 and M71) in J and K_S . In the following semester (2009A), we obtained observations of M5, but only in the J band due to poor weather conditions. In addition, K_S -band images of NGC 1851 that had been previously collected by two of us (G.B. and M.D.) using the VLT HAWK-I detector were included in the dataset.

All of our CFHT observations aimed to reach a signal-to-noise ratio of 25 at ~ 2.5 magnitudes below the main sequence turn-off (MSTO) of each cluster. To accomplish this, a series of long exposures, together with several short-exposure images (which were critical for the calibration of our fields to 2MASS photometry), were taken in the J and K_S filters for each cluster on our target list. By taking a series of exposures, each star was detected multiple times, thereby helping to improve the precision of the final photometry. We direct the reader to Table 1

which lists the image properties of each cluster. Unlike optical photometry, where one would separately observe standard star fields, the 2MASS All-Sky Point Source Catalog contains enough stars in each of our clusters which can be used as standards. For example, M13 has 3221 stars in the 2MASS All-Sky Point Source Catalog within 30 arcmin of its center. Of these, we selected stars with the lowest claimed photometric errors (typically errors < 0.02) for the calibration of our frames.

In addition to the on-target images, it was necessary to obtain a large number of off-target images of the sky because both the spatial and temporal variations of atmospheric emission in the IR are quite considerable ($\sim 10\%$ over a timespan of as little as 10 minutes). Indeed, particular care was taken in determining how to construct and subtract a sky image from a target image, since the quality of a processed image is dominated by precisely how this subtraction is carried out. In order to minimize the effects of the variable sky on our photometry, we decided to image an equal number of sky frames off-target as science frames on-target. We also chose to employ a large dither pattern so as to remove bad pixels when median combining the frames. Once observed, images were pre-processed by CFHT staff using the WIRC*am* pipeline. This included flat fielding, bias and dark subtraction, as well as sky subtraction.

Upon receiving the pre-processed images, instrumental magnitudes for all stars were obtained using the point spread function (PSF) modeling and fitting techniques in the DAOPHOT/ALLSTAR/ALLFRAME packages (Stetson 1987, Stetson & Harris 1988). In essence, these programs work by detecting stars on a specific image, building a model PSF from a few isolated, bright stars and then subtracting this PSF from all stars detected. (For a more detailed description of how these programs work, see Stetson 1987.) The standard star calibration directly to 2MASS stars in the same frame, was done by solving for the zero point, and colour terms which accounts for the difference in the central wavelengths of the CFHT and 2MASS J , and K filters.

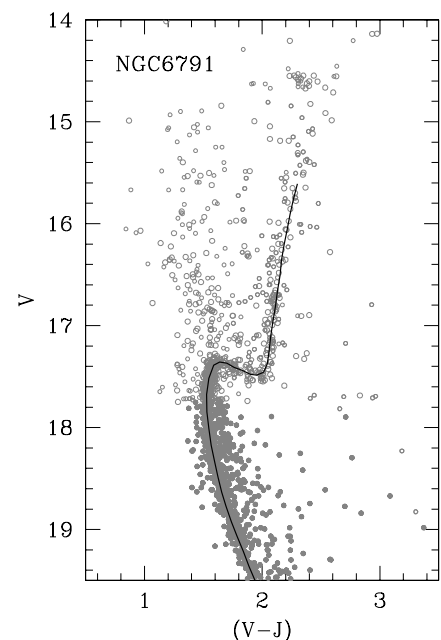


FIG. 2.— The derived $V-(V-J)$ fiducial sequence of NGC 6791 overlaying CFHT (filled circles) and 2MASS (open circles) photometry.

Cluster	Dates of Observations	Exposure time in J	Exposure time in K	Weather Conditions
M15	Aug 10-18, 2008	45s x 40, 5s x 7	20s x 97	photometric
M92	Aug 10-18, 2008	25s x 5, 45s x 14, 5s x 21	20s x 127, 5s x 19	photometric
M13	Aug 11-12, 2008	45s x 25	20s x 153	photometric
M5	June 11, 2009	20s x 56	...	photometric
NGC 1851	Jan 30, 2008	...	10s x 139	photometric
M71	Aug 10-18, 2008	5s x 22	5s x 45	photometric
NGC6791	Aug 10-18, 2008	5s x 21	...	photometric

TABLE 1
DESCRIPTION OF OBSERVATIONS FOR EACH TARGET.

One can check the overall quality of our transformed magnitudes by comparing stars in common between our fields and the 2MASS catalog. One example of such a comparison is shown in Figure 1 for NGC1851, where the differences between the standard 2MASS magnitudes and our final calibrated ones are plotted against both magnitude and colour. Reassuringly, the horizontal lines corresponding to zero difference appear to pass through the densest concentration of points in all plots. Moreover, there seem to be no strong systematic trends as a function of colour that would indicate the need for higher order colour terms in the photometric solutions.

To produce the CMDs, our final photometry for each cluster was combined with V -band data (see Stetson 2000; Stetson 2005). Our CMD of NGC1851, which is from VLT observations, extends from near the RGB tip to ~ 3 magnitudes below the MSTO. For the remaining six clusters, which were observed using the CFHT, we were able to obtain observations only for magnitudes fainter than the base of the RGB. The upper giant-branch stars were saturated in all of our frames, despite observing the target clusters with the shortest exposures possible on WIRCam. This problem occurred mainly because the seeing was 0.3 to 0.5'' better than we had requested during the nights

of observation, which resulted in a more concentrated PSF.

Thus, in order to populate the RGBs of the clusters that were observed using the CFHT, we queried the 2MASS catalog for all of the stars within 30' of the center of each cluster. With a photometric sensitivity of 10 sigma at $J=15.8$ and $K_S=14.3$ mag, 2MASS observations extend at least to the base of the giant branch for each of our target clusters. The 2MASS photometry for the selected giant-branch stars in each system (Skrutskie et al. 2006) was then combined with V -band photometry for the same stars (Stetson 2000; Stetson 2005).

Although it is ideal to have homogeneous observations for the entire range in cluster magnitude, the zero-points of our WIRCam photometry were set using 2MASS observations from the same catalog that was used to identify the RGB stars. Therefore, in principle, one should expect that there are no differences between these observations. However, in practice, the possibility that uncertainties in the zero-points may be appreciable should be kept in mind when employing the resultant CMDs and fiducial sequences. A list of our observed clusters and our adopted reddening and distance moduli are given in Table 2.

2.1. Fiducials

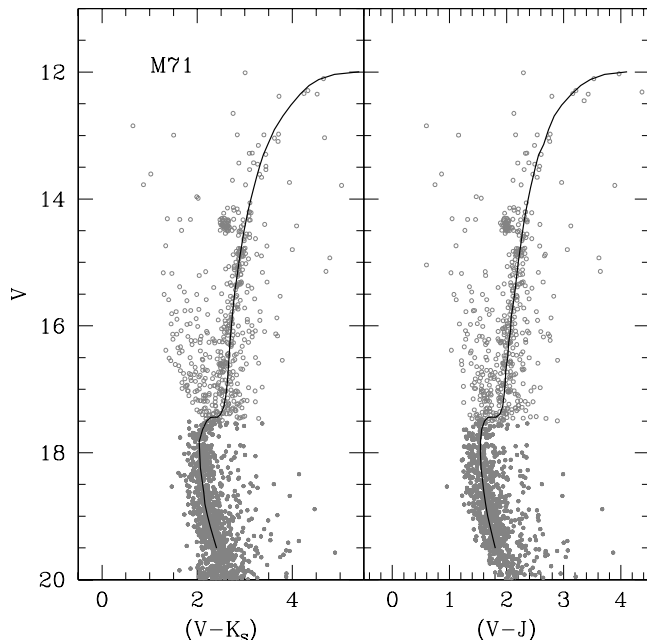


FIG. 3.— The derived $V-(V-K_S)$ and $V-(V-J)$ fiducial sequences of M71 overlaying CFHT (filled circles) and 2MASS (open circles) photometry.

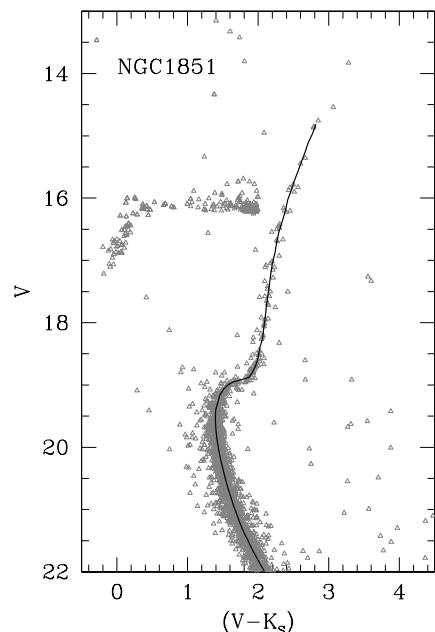


FIG. 4.— The derived $V-(V-K_S)$ fiducial sequence of NGC1851 overlaying HAWK-I K_S photometry.

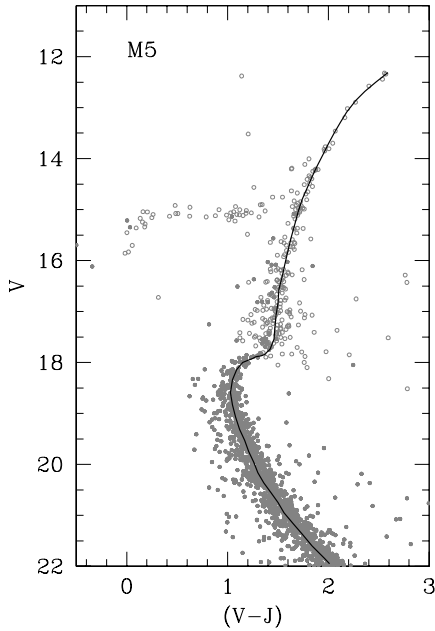


FIG. 5.— The derived $V-(V-J)$ fiducial sequence of M5 overlaying CFHT (filled circles) and 2MASS (open circles) photometry.

Fiducial sequences are ridge lines of the stellar loci in colour-magnitude space. The definition of these fiducials from cluster photometry is often based on visual inspection of the CMD, since automated scripts typically give poor results in regions of low star counts and where the magnitude varies weakly with colour, such as the subgiant branch (SGB). Moreover, contamination from field, AGB, binary, and horizontal-branch (HB) stars can significantly skew the the computed locus. For these reasons, we have derived all fiducials by dividing the magnitude axis into small bins (typically ~ 0.15 mag wide, or smaller in regions of nearly constant magnitude) and then calculating the median colour of those stars which we judge to belong to the cluster.

We present our observed CMDs in Figures 2–8 with 2MASS, CFHT/WIRCam, and VLT/HAWK-I photometry plotted as open circles, filled circles, and open triangles, respectively. Overlaid on the colour-magnitude diagrams are the derived fiducial sequences spanning the MS, SGB, and RGB (see Tables 2–9). In the case of M13, M92, and M15, there were insufficient points to define the fiducial for the subgiant branch; consequently, the latest Victoria-Regina Models by Vandenberg et al. (in preparation) of the same metallicity of each cluster were used to define the transition from the MS to the lower RGB in these cases (such points are marked with an asterisk in the tables).

3. TESTING THE COLOUR- T_{eff} RELATIONS USING OBSERVATIONS OF FIELD SUBDWARFS AND STAR CLUSTERS

Transforming isochrones from the theoretical $\log T_{\text{eff}}-M_{\text{bol}}$ plane to an observed CMD is accomplished through the use of colour- T_{eff} relations to link the fundamental stellar parameters to photometric indices. In this section, we investigate two recently developed colour transformations. The first of these is an empirical relation developed by Casagrande et al. (2010)

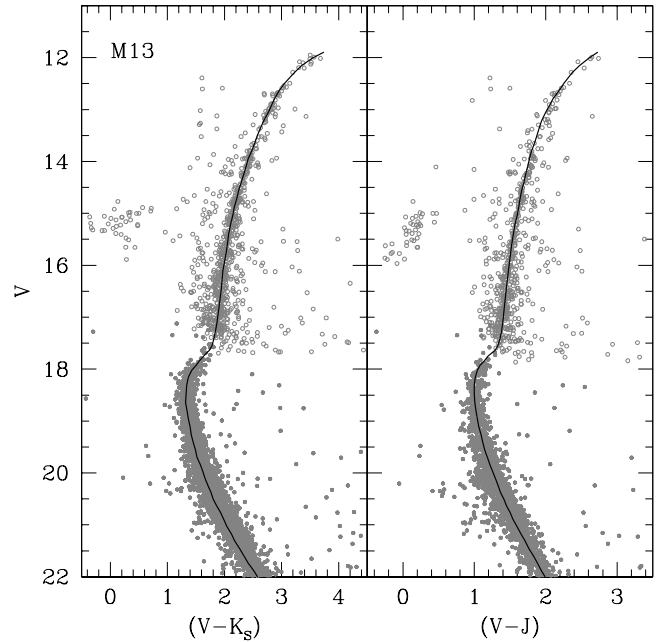


FIG. 6.— The derived $V-(V-K_S)$ and $V-(V-J)$ fiducial sequences of M13 overlaying CFHT (filled circles) and 2MASS (open circles) photometry.

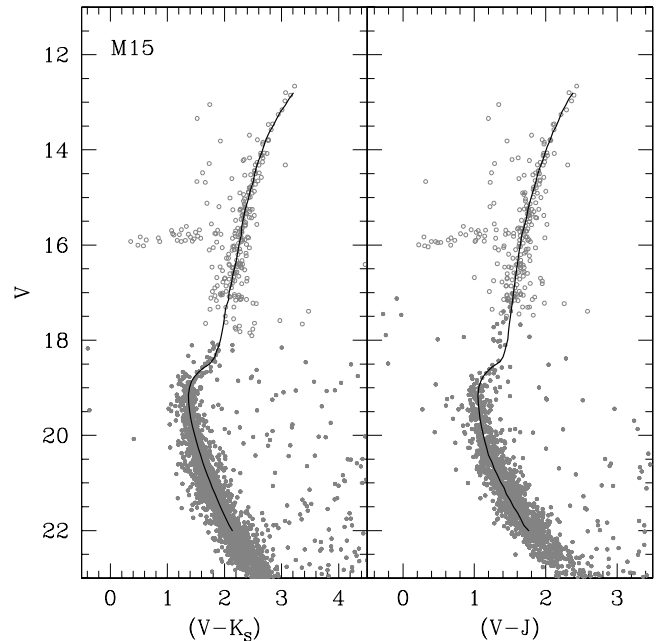


FIG. 7.— The derived $V-(V-K_S)$ and $V-(V-J)$ fiducial sequences of M15 overlaying CFHT (filled circles) and 2MASS (open circles) photometry.

Cluster	Type	α	δ	[Fe/H]	(m-M) _V	E(B-V)
M15	globular	21:29:58	+12:10:01	-2.4	15.29	0.108
M92	globular	17:17:07	+43:08:12	-2.4	14.62	0.023
M13	globular	16:41:41	+36:27:37	-1.60	14.40	0.016
M5	globular	15:18:36	+02:05:00	-1.40	14.45	0.038
NGC 1851	globular	05:14:06	-40:02:50	-1.40	15.50	0.034
M71	globular	19:53:46	+18:46:42	-0.80	13.78	0.220
NGC 6791	open	19:20:53	+37:46:30	+0.3	13.57	0.150

TABLE 2
PROPERTIES OF THE GALACTIC STAR CLUSTERS IN OUR SURVEY.

(hereafter referred to as CRMBA) who have applied the IRFM to a large sample of dwarf and subgiant stars of varying metallicity. They present their results as a set of polynomials which relate many photometric indices to T_{eff} and [Fe/H]. This empirical colour- T_{eff} relation has the advantage of being largely model independent, but it has the limitation of being applicable only to dwarf and SGB stars.

The second relation was derived by one of us (L.C.) from synthetic spectra based on the latest MARCS model atmospheres (Gustafsson et al. 2008) using the procedures described in VCS10, with the 2MASS filter transmission curves, absolute calibration and zero-points reported in Casagrande, Portinari & Flynn isochrones (VandenBerg et al. in preparation) using the MARCS and CRMBA colour- T_{eff} relations and test how well they are able to reproduce the observed VJK_S colours of field subdwarfs and our cluster photometry. Whenever possible, distances derived from *Hipparcos* parallaxes, along with the most up-to-date estimates of the cluster metallicities, have been assumed. However this study is much less concerned with the absolute fit of the isochrones to the observed CMDs than with the extent to which a *consistent* interpretation of the same cluster can be found on different colour planes. Since any inaccuracies in distance moduli or [Fe/H] should be evident in *all* colour planes, they should not effect our overall conclusions (though the possibility that chemical abundance anomalies may be present, and that they might affect the fluxes in some filter bandpasses more than others should be kept in mind). This does, of course, have the caveat that the observations must be free from systematic errors and that the extinction in all colour bands is accurately determined.

In the following analysis we transform the latest Victoria and CRMBA colour- T_{eff} relations and test how well they are able to reproduce the observed VJK_S colours of field subdwarfs and our cluster photometry. Whenever possible, distances derived from *Hipparcos* parallaxes, along with the most up-to-date estimates of the cluster metallicities, have been assumed. However this study is much less concerned with the absolute fit of the isochrones to the observed CMDs than with the extent to which a *consistent* interpretation of the same cluster can be found on different colour planes. Since any inaccuracies in distance moduli or [Fe/H] should be evident in *all* colour planes, they should not effect our overall conclusions (though the possibility that chemical abundance anomalies may be present, and that they might affect the fluxes in some filter bandpasses more than others should be kept in mind). This does, of course, have the caveat that the observations must be free from systematic errors and that the extinction in all colour bands is accurately determined.

As previously mentioned, this paper provides an extension of the $BV(RI)_C$ study by VCS10 to the near-IR. Consequently, we have tried to ensure that the analysis of the colour transformations for a given cluster is consistent across optical and infrared colours by employing identical isochrones (i.e., for the same age and metallicity) and by adopting the same values of the reddening and distance modulus (in the case of clusters which are in common with VCS10: M67, NGC 6791, NGC 1851, M5, M92). Additionally, the V -band photometry of the clusters presented in the following sections is from the same catalogues (Stetson 2000; Stetson 2005) that were used for the comparisons presented by VCS10.

The extinction coefficients adopted in this work are $E(V-J)/E(B-V)=2.25$, $E(V-K_S)/E(B-V)=2.76$ and $E(V-H)/E(B-V)=2.55$ (McCall (2004)).

3.1. M67 ([Fe/H] \approx 0.0)

M67 is a particularly well studied, relatively nearby open cluster, with a metallicity that is very close to solar, according to the results of high-resolution spectroscopy (Tautvaišienė et al.

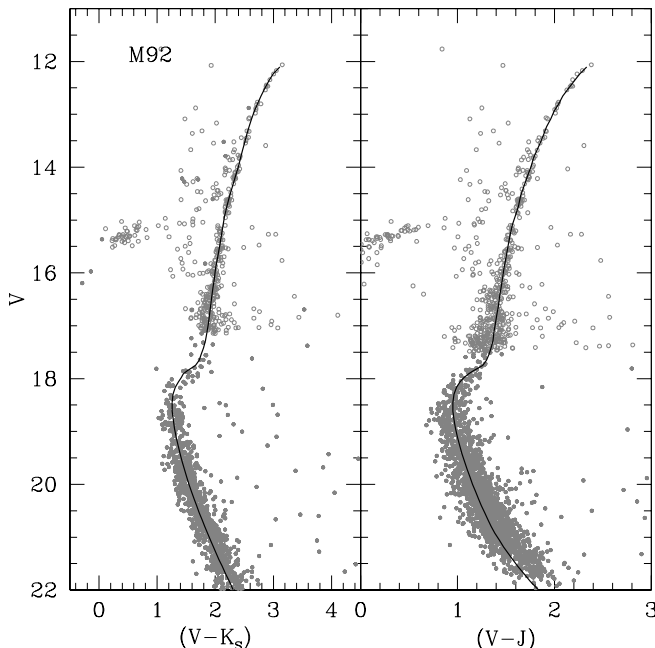


FIG. 8.— The derived $V-(V-K_S)$ and $V-(V-J)$ fiducial sequences of M92 overlaying CFHT (filled circles) and 2MASS (open circles) photometry.

2000; Randich et al. 2006). See VCS10 for a summary of its basic properties, together with supporting references. Because of its proximity, 2MASS JHK_S observations of M67 reach well below the MSTO; consequently, the CMDs shown in Figure 9 could be produced simply by combining M67 data from 2MASS (Skrutskie et al. 2006) with the latest reduction of the V -band photometry discussed by Stetson (2005). The isochrone in this figure is that for an age of 3.7 Gyr from Michaud et al. (2004), and just as VCS10 found from their comparisons of the same isochrone with $BV(RI)_C$ photometry, both the MARCS and CRMBA transformations to the $V-J$ and $V-K_S$ colour planes enable the models to match the observed photometry exceptionally well over the entire range of luminosity that has been plotted. Indeed, the differences between the two colour- T_{eff} relations are barely discernible. (Only in the case of M67 have we compared theory and observations on a $[(V-H)_0, M_V]$ -diagram. Although the isochrone fits the data quite well, there is a slight, apparently nearly constant offset between the two, which may be due to a small error in our assumed value of $E(V-H)$ or in the zero-point of the H magnitudes derived from the MARCS model atmospheres.)

3.2. NGC 6791 ($[Fe/H] \approx +0.3$)

Being the most metal rich cluster in our sample (and only open cluster for which we have collected JK_S observations), NGC 6791 provides an important test of the colour- T_{eff} relations applicable to super-metal-rich stars. Here we have adopted the recent $[Fe/H]$ estimate from Boesgaard et al. (2009). This is consistent with Brogaard et al. (2010) who derived $[Fe/H] = 0.29 \pm 0.03$ (random) ± 0.07 (systematic) in their spectroscopic analysis. Anthony-Twarog et al. (2007) have noted that the Carraro et al. (2006) determination of $[Fe/H] = +0.38$ for NGC 6791 should be reduced to $\sim +0.28$ (hence in very good agreement with the Brogaard et al. result) if those authors

had adopted $E(B-V) = 0.15$ in their analysis, instead of 0.09.

Because of its large distance and low Galactic latitude, reddening estimates of NGC 6791 vary considerably in the literature. As discussed by Chaboyer, Green, & Liebert (1999), the derived reddenings for NGC 6791 span the range $0.09 \leq E(B-V) \leq 0.26$. Kuchinski et al. (1995) have used subdwarf-B stars to provide a tight constraint on the reddening, finding $E(B-V) = 0.17 \pm 0.01$. This agrees well with the Schlegel et al. (1998) estimate of $E(B-V) = 0.155$ mag, which is also favoured by the comparison of the NGC 6791 CMD with that for solar neighborhood stars from *Hipparcos* data (see Sandage, Lubin, & Vandenberg 2003). Additionally, Brogaard et al. (2010) also derived $E(B-V) = 0.160 \pm 0.025$, which adds to the support of our adopted reddening of 0.15.

In consistency with VCS10, we adopt a distance modulus of $(m-M)_V = 13.57$ which was found through a fit of the cluster CMD to local field dwarfs having metal abundances in the range $+0.15 \leq [Fe/H] \leq +0.45$ and $\sigma(M_V) \leq 0.15$ (based on *Hipparcos* parallaxes). Figure 10 shows our $[(V-J)_0, M_V]$ CMD for dwarf and SGB stars in NGC 6791 is well reproduced by either the MARCS- or CRMBA-transformed Victoria isochrone on the assumption of the aforementioned reddening and distance. (Only along the upper RGB does the isochrone seem to deviate to the blue of the observations, which is consistent with the possibility that the MARCS atmospheres have insufficient blanketing in cool super-metal-rich stars.) Thus, there is excellent consistency with the isochrone fits reported by VCS10 to the $[(B-V)_0, M_V]$ - and $[(V-I)_0, M_V]$ -diagrams of NGC 6791. Since $E(V-J) = 2.25 E(B-V)$ (e.g., McCall 2004), this consistency provides a further (strong) argument that the foreground reddening must, indeed, be quite close to $E(B-V) = 0.15$. This example thus provides an instructive example of how valuable it is to have both optical and near-IR photometry to constrain the reddening in the case of highly reddened systems.

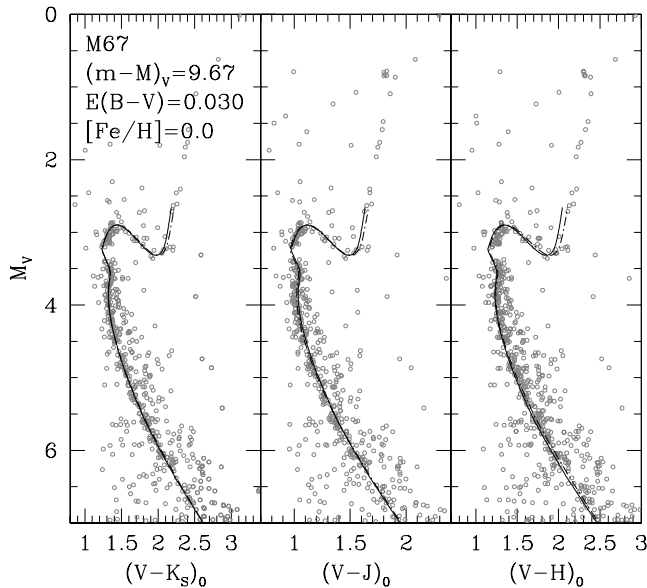


FIG. 9.— Comparison of a 3.7 Gyr isochrone for $[Fe/H] = 0.0$ with 2MASS/Stetson $V-K_S$, $V-J$, and $V-H$ observations of M67. The solid and dot-dashed curves assume the MARCS and Casagrande et al. (2010) colour transformations, respectively.

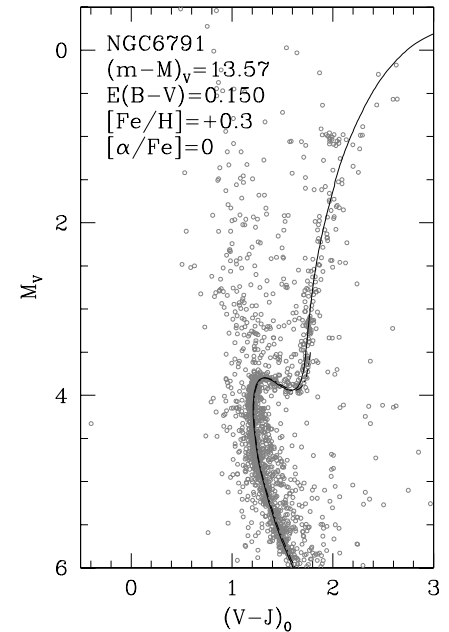


FIG. 10.— Comparison of an 8.0 Gyr isochrone for $[Fe/H] = +0.3$ and $Y = 0.30$ with our $V-J$ observations of NGC 6791. The solid and dot-dashed curves assume the MARCS and Casagrande et al. (2010) colour transformations, respectively.

3.3. M71 ($[Fe/H] \approx -0.75$)

M71 represents the metal-rich end of our sample of globular clusters (GCs). We adopt an $[Fe/H] = -0.80$ as derived by Boesgaard et al. (2005). It is quite obvious from the CMD in Figure 3 that this cluster has a low Galactic latitude, as contamination from field stars is still significant even when only those stars contained within an annulus of ~ 7 arcmin around the cluster center are plotted. Furthermore, the Schlegel et al. (1998) dust maps indicate that the reddening is differential across the cluster, which contributes to the spread in colour at any given magnitude, thereby hindering the definition of tight photometric sequences for this cluster in any photometric band.

As far as the cluster distance is concerned, we have adopted a distance modulus that leads to the most consistent interpretation between M71 (in this paper), and that of 47 Tuc (in VCS10), which is known to have very close to the same metallicity. If the latter has $(m-M)_V = 13.40$, as assumed by VCS10, and if the difference in magnitude of the HBs of 47 Tuc and M71 is as given by Hodder et al. (1992), then a value of $(m-M)_V = 13.78$ is obtained for M71.

Because of its low Galactic latitude ($b = -4.6^\circ$), M71 poses a challenge for reddening determinations: estimates in the literature range from $E(B-V) = 0.21$ to 0.32 (e.g. Kron & Guetter 1976; Harris 1996).

Figure 11 shows the isochrones compared with our observations. The observations are matched well by isochrones on the $[(V-K_S)_0, M_V]$ -plane using either the MARCS or CRMBA colour transformations. In the case of the $V-J$ observations, the isochrones match the base of the RGB well, but drift to the blue side of the lower MS, and to the red of the upper MS. However, the discrepancies at the faintest magnitudes may have an observational origin given that they arise close to the photometric limit of J . It should be noted that the reddening adopted here, $E(B-V) = 0.20$ was chosen to obtain a fit to the $B-V$ photom-

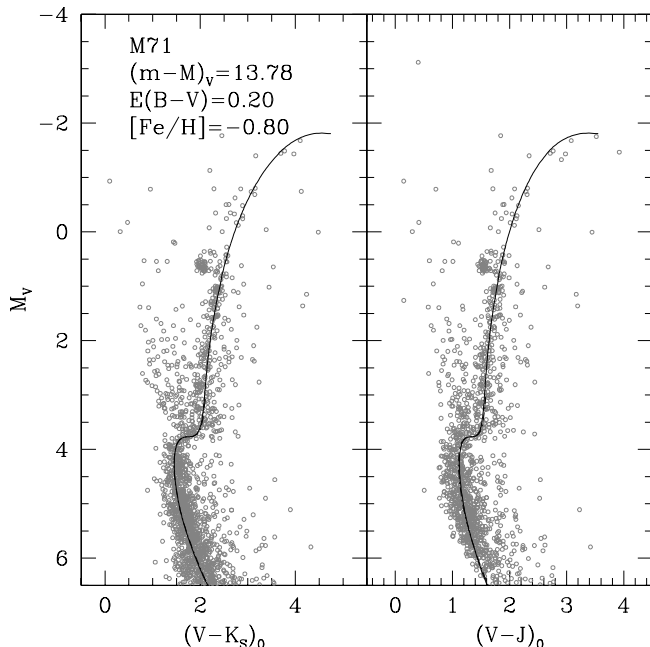


FIG. 11.— Comparison of an 11 Gyr isochrone for $[Fe/H] = -0.75$, with our observations of M71. The solid and dot-dashed curves assume the MARCS and Casagrande et al. (2010) colour transformations, respectively.

etry. Thus, the models provide consistent interpretations across the $B-V$, $V-J$ and $V-K$ colour-planes.

3.4. M5 and NGC 1851 ($[Fe/H] \approx -1.4$)

As discussed quite extensively by VCS10, when Schlegel et al. (1998) reddenings are applied to the observed stars in M5 and NGC 1851 and then their CMDs are shifted in the vertical direction so that the red HB populations of the two clusters have the same luminosities, one finds that the main-sequence fiducials of both clusters superimpose one another nearly perfectly, suggesting a common metallicity. This conflicts with the results of most spectroscopic studies, which indicate that NGC 1851 is ≈ 0.2 dex more metal-rich than M5 (e.g., Carretta et al. 2009; Kraft & Ivans (2003)). If this is correct, the latter should have a slightly brighter HB than the former, and therefore a slightly brighter MS at a given color — but this would be inconsistent with the assumed difference in $[Fe/H]$ (unless Y or the heavy-element mixture also varies). However, a resolution of this issue is not important for the present investigation, which seeks to determine if consistent interpretations of the photometry across all colour planes can be found. Following VCS10, we adopt $[Fe/H] = -1.4$ for both M5 and NGC 1851 which is the metallicity which tends to be favoured by stellar models such as Vandenberg (2000) (see VCS10 for a detailed description on this choice of metallicity).

In Figure 12, we overlay the same 11 Gyr isochrone used by VCS10 in their study of $BV(RI)_C$ photometry, onto the $[(V-K_S)_0, M_V]$ -diagram of NGC 1851. For consistency with VCS10, we have adopted the same reddening and distance modulus; specifically, $E(B-V) = 0.034$ (Schlegel et al. 1998) and $(m-M)_V = 15.50$, based on observed and predicted HB luminosities (Vandenberg et al. 2000) as well as MS-fits of cluster fiducials to the CRMBA-transformed isochrones (and hence to the subdwarf standards for which these relations are defined;

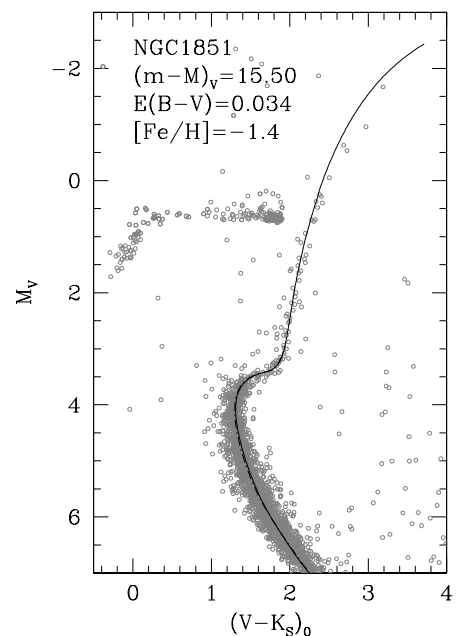


FIG. 12.— Comparison of an 11 Gyr isochrone for $[Fe/H] = -1.4$, $[\alpha/Fe] \approx 0.4$, and $Y = 0.25$ with our $V-K_S$ observations of NGC 1851. The solid and dot-dashed curves assume the MARCS and Casagrande et al. (2010) colour transformations, respectively.

VCS10). We find that isochrones using the MARCS colour- T_{eff} relations, or the CRMBA transformations for dwarf/SGB stars, are able to reproduce our $V-K_S, V$ photometry of NGC 1851 rather well, except for the upper RGB (where there are few stars and where the stellar images are approaching the saturation limit). These results are fully consistent with those found by VCS10 when they analyzed $V-I, V$ data. However, as they reported, the giant branch of the isochrone on the $[(B-V)_0, M_V]$ -diagram is significantly bluer than the observed RGB. Thus, only the MS stars can be consistently fitted on all of the colour planes that have been considered.

In the case of M5, we have assumed that $E(B-V) = 0.038$ and $(m-M)_V = 14.45$ (see VCS10), which results in the comparison of the MARCS- and CRMBA-transformed isochrones with the $V-J$ observations shown in Figure 13. (Note that the isochrones are identical to those fitted to NGC 1851 photometry.) Given the differences in the relative positions of the RGBs of M5 and NGC 1851 noted above, it is not surprising to find that, since the MARCS models are able to reproduce the giant branch of NGC 1851 in $V-K_S$ and $V-I$, they lie to the red of the observed RGB of M5 in $V-J$ and $V-I$ (see VCS10, who also show that the predicted giant branch matches the $B-V$ colours of M5 giants quite well). As far as the main sequence of M5 on the $[(V-J)_0, M_V]$ -diagram is concerned, the isochrones lie slightly blueward of the lower MS, and to the red of the upper MS, as seen in M71. As discussed below, this is also seen in the case of M15 and M92, and perhaps indicates that there is a small problem with the transformations to $V-J$.

3.5. M13 ($[Fe/H] \approx -1.6$)

For our comparisons with M13, we have selected isochrones with $[Fe/H] = -1.6$ based on the work of Kraft & Ivans (2003). This is within 0.05 dex of the long favoured Zinn & West (1984) value of -1.65 and within 0.02 dex of the recent Carretta et al. (2009) value of -1.58 . We have also adopted $(m-M)_V = 14.40$ which is very close to the value obtained by Grundahl, Stetson, & Andersen

(1998) from a fit of Stromgren photometry to metal-poor subdwarfs with Hipparcos parallaxes, who also assumed $[Fe/H] = -1.6$. Additionally, Paltrinieri et al. (1998) derived $\delta(V)$ between M3 and M13 of 0.64 mag - so if M3 has 15.00 (as adopted in VCS10), then 14.40 is implied for M13 from the Paltrinieri et al result (if the 0.01 mag difference in reddening is taken into account). We adopt $E(B-V) = 0.016$ from Schlegel et al. (1998).

In figure 14, we compare a 12 Gyr isochrone with our VJ and VK_S photometry, finding that (for both colours) the isochrones provide a good match to the observed MS, but not to the observed RGB, which is significantly bluer at a fixed magnitude than the predicted colours. This is also found when fitting VI data (not shown here); i.e., when the same isochrones are overlaid onto $V-I, V$ photometry, the main sequence is well matched but the predicted giant branch is offset to the red of the observed RGB. Interestingly, no such problem is found fitting the VI (or BV) photometry of M3 (see VCS10), which is thought to have close to the same metal abundance as M13.

3.6. M15 and M92 ($[Fe/H] \approx -2.4$)

M15 and M92 constitute the most metal poor clusters in our sample. For both clusters, a metallicity near $[Fe/H] = -2.4$ is consistent with the latest results from high-resolution spectroscopy (Kraft & Ivans 2003; Carretta et al. 2009). As regards their distances, we have adopted $(m-M)_V = 14.62$ for M92 (see Vandenberg et al. (2002)), and $(m-M)_V = 15.29$ for M15 given that Durrell & Harris (1993) have found that the main sequences of both clusters will superimpose one another if a vertical shift of 0.67 mag is applied to the M92 CMD once their turnoff colours are matched. According to Schlegel et al. (1998), the reddenings of M92 and M15 are $E(B-V) = 0.023$ and 0.108 mag, respectively.

As shown by VCS10, a MARCS-transformed isochrone for 13.5 Gyr and $[Fe/H] = -2.4$ provides a reasonably good fit to

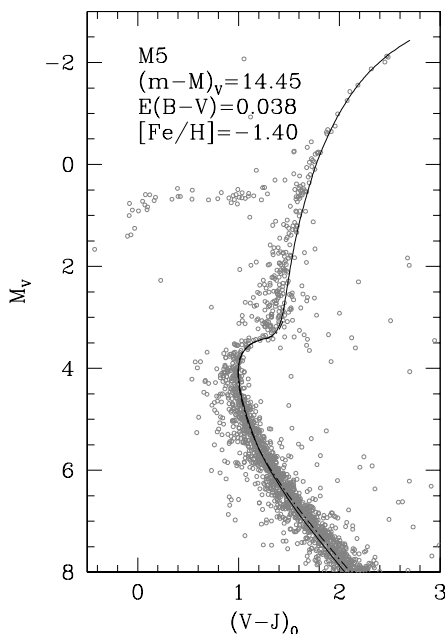


FIG. 13.— As in the previous figure, except that the (same) isochrone is compared with our $V-J$ observations of M5.

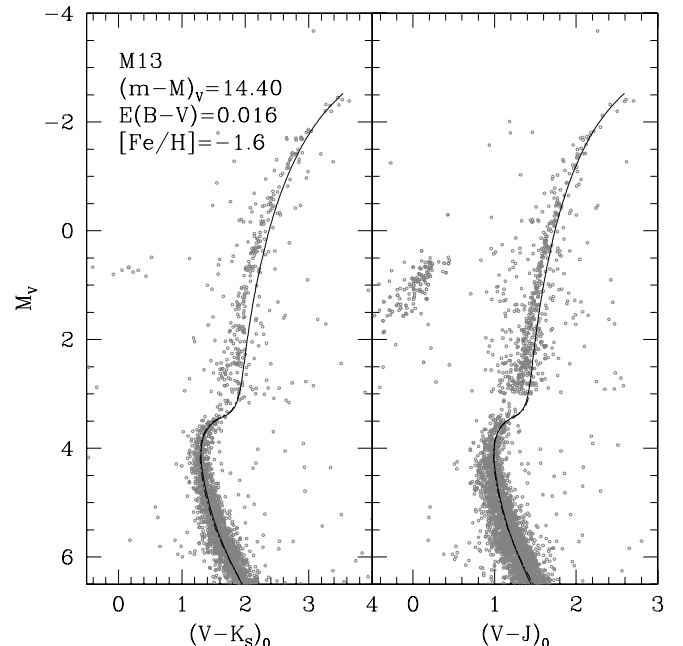


FIG. 14.— Comparison of a 12 Gyr isochrone for $[Fe/H] = -1.60$ with our observations of M13. The solid and dot-dashed curves assume the MARCS and Casagrande et al. (2010) colour transformations, respectively.

both the BV and VI photometry of M92 — aside from the fact that a small colour shift must be applied to the $V-I$ colours in order to obtain consistent fits to the various CMDs that can be generated from $BV(RI)_C$ photometry. Their additional observation that the isochrones tend to deviate to the blue side of the observed lower MS is apparently seen in especially the $[(V-J)_0, M_V]$ -diagrams of M15 and M92 as well (see Figures 15 and 16). We have no explanation for such deviations, which appear to be most pronounced in the VJ photometry for M15.

Perhaps the most serious concern is that, in both the $V-J$ and $V-K_S$ colour planes, the isochrones lie consistently to the red of the observed RGBs of M15 and M92. Near the base of the giant branch, the offsets amount to ~ 0.12 mag in $V-K_S$ and ~ 0.09 mag in $V-J$ and the typical error in the photometry (~ 0.02 mag) cannot explain these colour offsets. Surprisingly, VCS10 find that the same isochrones provide a good fit to optical CMDs, apart from the small, constant offset between the predicted and observed RGB on the $[(V-I)_0, M_V]$ -plane previously mentioned. Since we are using the same V -band photometry as VCS10, one might question the accuracy of the J and K_S photometry for M15 and M92. However, this is not a viable explanation because the near-IR photometry for the cluster giants, as with all our CFHT clusters, comes directly from 2MASS, and such a large zero-point offset is highly unlikely. Indeed, because the isochrones reproduce $BV(RI)_C$ observations quite well, one wonders whether there is a problem with the synthetic J and K_S magnitudes that are derived from MARCS model atmospheres, though we have no other reason to question these results. Further work is clearly needed to understand this puzzle.

3.7. Field Subdwarfs ($-2.2 \lesssim [Fe/H] \lesssim -0.5$)

Subdwarfs are metal-poor stars with halo kinematics whose orbits have brought them into the solar neighbourhood. With

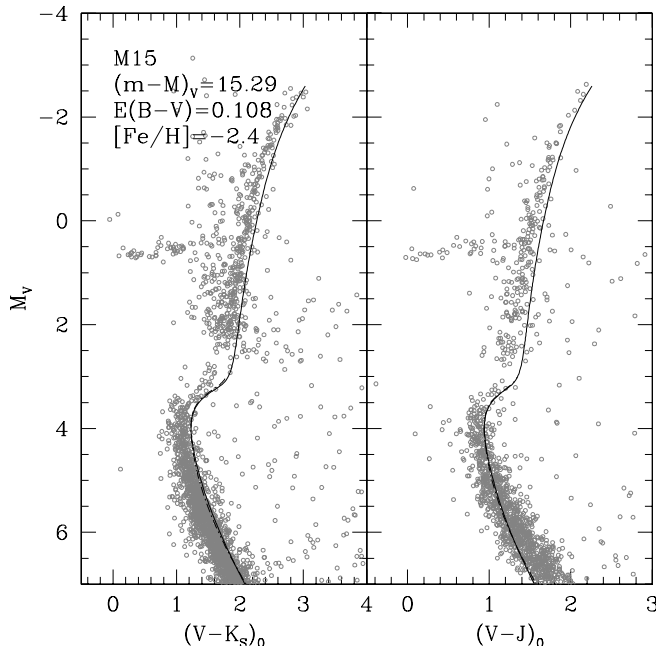


FIG. 15.— Comparison of a 13.5 Gyr isochrone for $[Fe/H] = -2.40$ with our observations of M15. The solid and dot-dashed curves assume the MARCS and Casagrande et al. (2010) colour transformations, respectively.

many of these stars having accurate distances determinations from *Hipparcos* and recent estimates of $\log g$, and $[Fe/H]$ based on high-resolution spectroscopy, they provide strong constraints on the T_{eff} scale of isochrones and colour- T_{eff} relations at low metallicities. In the following analysis, we use a sample of ~ 100 subdwarfs compiled by VCS10. The photometric and fundamental stellar properties (e.g., T_{eff} , $\log g$ and $[Fe/H]$) for the majority of these stars were taken from Table 8 of CRMBA with the addition of 4 stars from Clementini et al. (1999). For a further description on the properties and choice of this sample, see VCS10.

In figure 17 we show the level of agreement between the observed and predicted 2MASS colours, $(V-K_S)$, $(V-J)$, and $(J-K_S)$, of the subdwarfs in our sample. The predicted MARCS colours for each star are found by interpolating in tables of synthetic colours assuming the T_{eff} , $\log g$, and $[Fe/H]$ values given by CRMBA. For these colour-colour comparisons we use only MARCS transformations since the CRMBA relations are themselves based on most of the same stars used here, so they will necessarily yield colours that agree well, in the mean, with the observed photometry. As noted in the three panels of figure 17, offsets of ~ 0.01 mag to the blue for the predicted $(V-K_S)$ and $(J-K_S)$ are needed to achieve consistency with observations. The predicted $(V-J)$ colours show a very small mean offset of 0.001 mag from the observed colours, though the largest deviations occur for the reddest stars, which suggests (perhaps) that the transformations to $V-J$ for cooler dwarf stars may need some adjustment. (Recall that, although this evidence is based on very few cool subdwarfs with measured $V-J$ colours, similar problems were seen in our comparisons with the $V-J$ photometry for MS stars in the low metallicity clusters M92, M15, M13 and M5; see the previous subsections.)

While the comparisons described above are completely independent of stellar evolutionary models, instructive comparisons of the theoretical isochrones with the *Hipparcos* subdwarfs can also be carried out. By superimposing subdwarfs onto a grid of

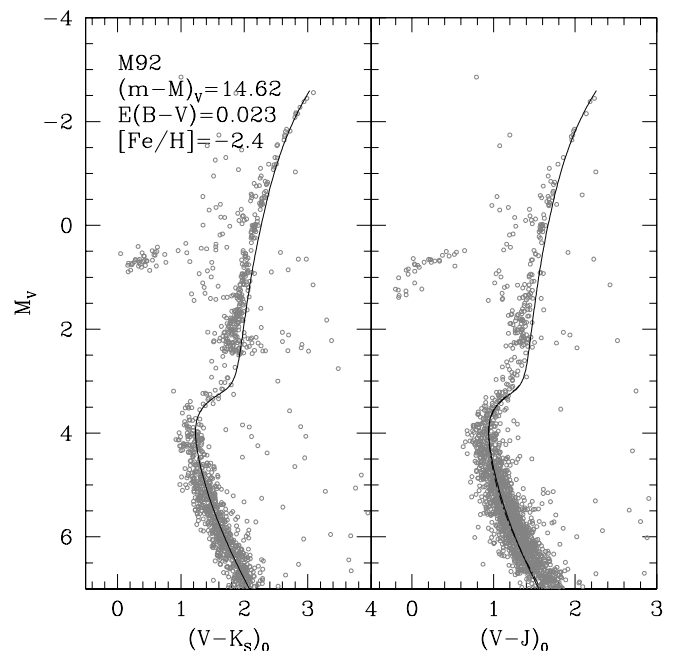


FIG. 16.— As in the previous figure, except that the (same) isochrone is compared with our observations of M92.

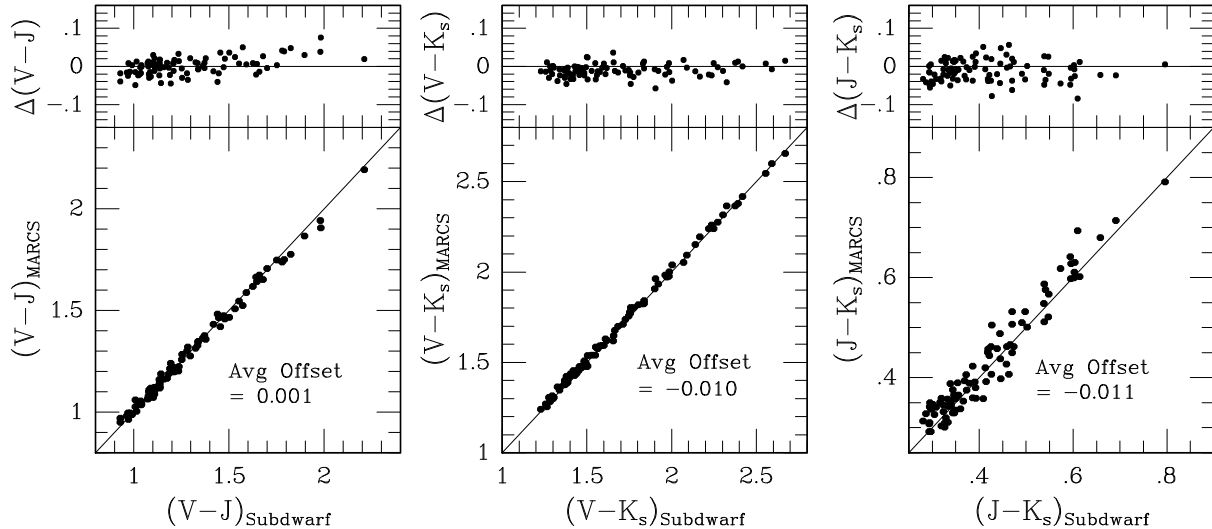


FIG. 17.— Comparison of the observed subdwarf colours with those predicted by MARCS colour transformations on the assumption of the T_{eff} , $\log g$ and $[\text{Fe}/\text{H}]$ determinations of CRMBA. The average offsets noted in each panel are relative to the observed colours. The upper panels plot the differences in the colours as a function of the subdwarf colours in the sense *observed minus predicted*.

isochrones for a wide range in $[\text{Fe}/\text{H}]$ (and a fixed age — though isochrones exhibit essentially no age dependence at faint luminosities), it is possible to examine the consistency of the observed $[\text{Fe}/\text{H}]$ values and colours with those inferred from the isochrones, given the observed temperatures. If a star lies on the same isochrone (say, one with $[\text{Fe}/\text{H}] = -1.5$) in all of the colour planes, one can conclude that the colour- T_{eff} transformations are consistent for those colours. If any obvious discrepancies exist for different filter combinations, then this is an indication of a problem with the colour-temperature relations for one or more colour indices (i.e., they do not adequately represent the spectrum of a star in the wavelength ranges spanned by the relevant filters).

In the lower panel of figure 18, we superimpose *Hipparcos* (van Leeuwen (2007)) subdwarfs onto 12 Gyr Victoria isochrones for $[\text{Fe}/\text{H}]$ values from -2.4 to -0.6 (in the direction from left to right) transformed into the $[(V-J)M_V]$ -, $[(V-K_S)M_V]$ - and $[(J-K_S)M_V]$ -planes using the MARCS transformations. For each subdwarf, the CRMBA estimate of its $[\text{Fe}/\text{H}]$ value minus the $[\text{Fe}/\text{H}]$ value of the isochrone on which the subdwarf is located is plotted in the middle panel, while the upper panel plots the difference between the observed subdwarf colour and that of the isochrone which has the same metallicity as the star (at the same M_V). These panels provide a measure of the quality of the fit to the observations. For example, if the isochrones were too red, most of the points would have positive $\delta[\text{Fe}/\text{H}]$ values and negative $\delta(\text{colour})$ values. Figures similar to 18 and 19, but for the $(B-V)$, $(V-R)$, and $(V-I)$ colour planes, are given in the study by VCS10, where the individual subdwarfs are identified.

The subdwarfs in the $V-K_S$ and $V-J$ colour planes show significant relative shifts with respect to the isochrones (i.e.,

the subdwarfs do not lie on the same position relative to the same isochrone in both colours). However, the scatter on the $\delta[\text{Fe}/\text{H}]$ and $\delta(\text{colour})$ planes is quite symmetric overall in both $V-K_S$ and $V-J$, with most of the redder stars having negative $\delta[\text{Fe}/\text{H}]$ and positive $\delta(\text{colour})$ values, whereas most of the bluer stars have positive $\delta[\text{Fe}/\text{H}]$ and negative $\delta(\text{colour})$ values. Thus, the isochrones are consistent with the observations, in the mean, with only a slight trend in the sense that the isochrones are somewhat too blue for the redder stars and too red for the bluer stars.

A different conclusion is drawn regarding the $J-K_S$ transformations shown in the right panel of Figure 18; the MARCS-transformed isochrones imply implausibly low values of $[\text{Fe}/\text{H}]$, which are contrary to the implications from the other colour planes. When looking at the $\delta[\text{Fe}/\text{H}]$ and $\delta(\text{colour})$ plots in the upper panels, one finds that most of the points have positive $\delta[\text{Fe}/\text{H}]$ and negative $\delta(\text{colour})$ values, indicating that the isochrones are too red, in the mean, relative to the observations. The $J-K_S$ panels also indicate that there is no obvious trend with colour or with metallicity.

Figure 19 plots the same isochrones as in Figure 18, but transformed to the various colour planes using the CRMBA colour- T_{eff} relations. When comparing the subdwarf colours and metallicities with those of the isochrones, we find there is no obvious trend with either colour or metallicity, which indicates that the CRMBA-transformed isochrones agree well, in the mean, with the observations, while the absence of trends provides a verification that the functional form used in CRMBA transformations well represents the (bulk of) stars upon which it is built.

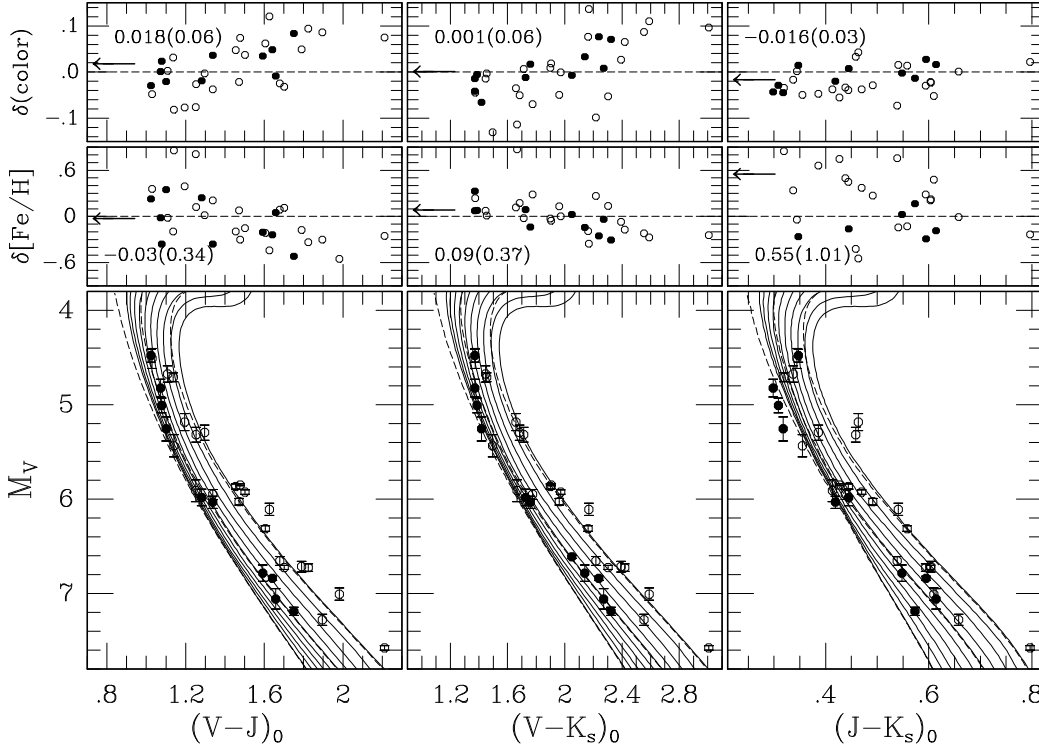


FIG. 18.— *Lower Panels:* Sample of Hipparcos subdwarfs overlying 12 Gyr Victoria isochrones in the $[(V-J)_0, M_V]$ -, $[(V-K_s)_0, M_V]$ - and $[(J-K_s)_0, M_V]$ -planes. The isochrones plotted here have $[\text{Fe}/\text{H}]$ values of -2.4 to -0.6 in increments of 0.2 dex, from left to right, and MARCS transformations have been used to transpose the models to the various CMDs. To demonstrate the age insensitivity for magnitudes $M_V \geq 4.5$, dashed lines show 10 Gyr isochrones for $[\text{Fe}/\text{H}] = -0.6, -1.4,$ and -2.4 . The photometry and metallicity of each subdwarf is taken from CRMBA, and the error bars represent 1σ uncertainties in the M_V values as derived from *Hipparcos* parallaxes. Subdwarfs having $[\text{Fe}/\text{H}] \leq -1.2$, as given by CRMBA, are plotted as filled circles, and those with higher metallicities are plotted as open circles. *Middle Panels:* Plotted as a function of colour, the difference between the CRMBA estimate of $[\text{Fe}/\text{H}]$ for each star and that inferred from the interpolated (or extrapolated when necessary) isochrone that matches its location on the colour- M_V diagram in the lower panel. The arrows and the numbers, together with the standard deviation (in parentheses), indicate the mean $\delta[\text{Fe}/\text{H}]$ for all of the subdwarfs that have been considered. *Upper Panels:* The difference in colour that would need to be applied to each subdwarf in order to achieve perfect consistency of its position relative to the isochrones in the lower panel. In this case, the arrows and numbers indicate the mean values of $\delta(\text{colour})$ for the subdwarf sample.

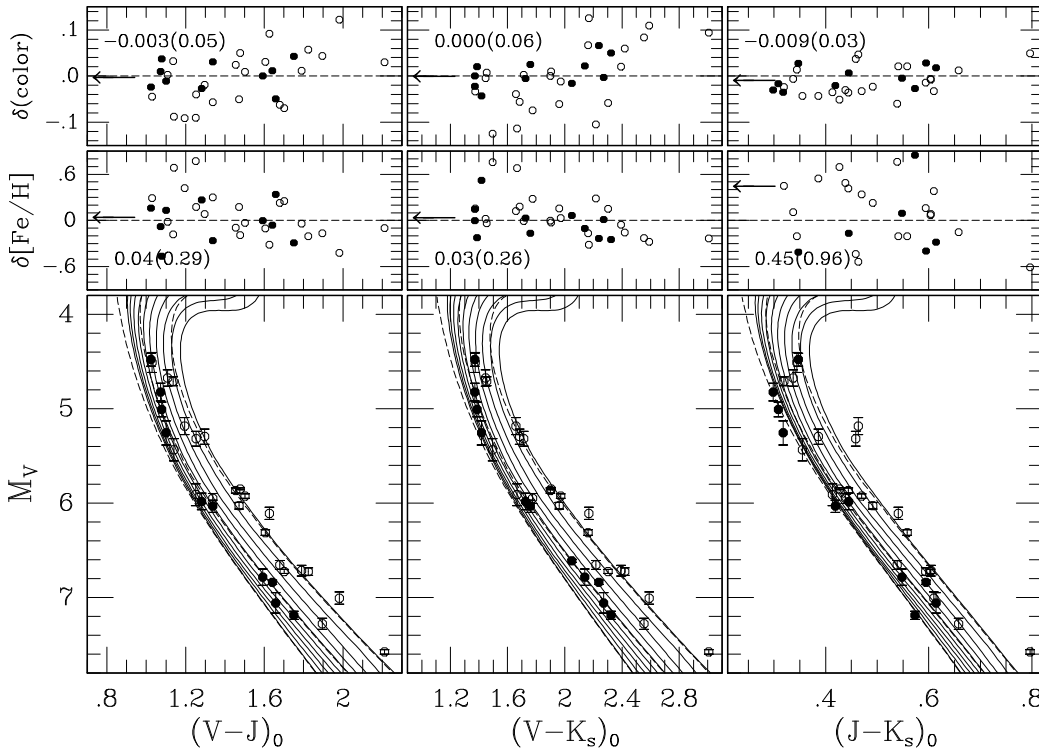


FIG. 19.— Similar to previous figure, except that the isochrones are transformed using the colour- T_{eff} relations developed by CRMBA.

We have derived fiducial sequences for the Galactic star clusters M15, M92, M13, M5, NGC 1851, M71, and NGC 6791 (encompassing $-2.4 \lesssim [\text{Fe}/\text{H}] \lesssim +0.3$) using near-IR observations obtained with the WIRCam imager on the Canada-France-Hawaii Telescope and the HAWK-I detector on the VLT. These fiducial sequences, which are presented in Figure 20 on the $[(V-J)_0, M_V]$ - and $[(V-K_S)_0, M_V]$ -planes, illustrate how the photometric properties of these old stellar populations vary as a function of $[\text{Fe}/\text{H}]$. With spectroscopic metallicity determinations and relative age estimates that are accurate to within ± 0.25 dex and ± 1.5 – 2 Gyr, respectively, these fiducials can, in principle, be used to photometrically determine the age and metallicity of resolved stellar systems. Unlike isochrone analyses, metallicity determinations made through comparisons with fiducials are independent of stellar evolutionary models. Hence, these fiducials provide a set of empirical isochrones that can serve as valuable tools for future stellar population investigations involving the 2MASS filters.

Based on these data, a summary of our results is as follows:

- (1) The predicted $V-J$, $V-K_S$, and $J-K_S$ colours given by the MARCS transformations for local subdwarfs agree well with those observed (i.e., to within ~ 0.01 mag) when the temperatures and metallicities of the latter are as given by CRMBA.
- (2) While isochrones appear to be too blue when compared with lower main sequence stars in metal-poor GCs on the $[(V-J)_0, M_V]$ -plane, no significant problems are found matching their $V-K_S$ colours.
- (3) Our analysis of cluster RGB stars indicates that the isochrones and the colour transformations faithfully reproduce the properties of metal-rich giants, but not those of lower metallicity. In

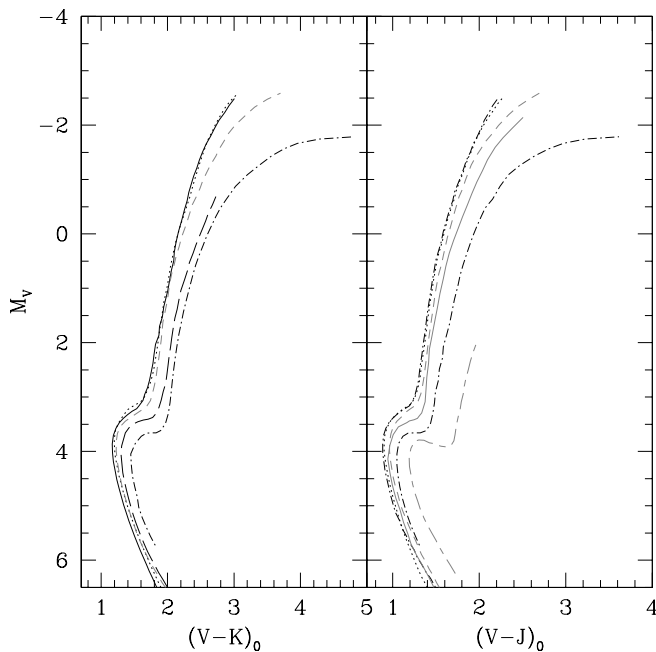


FIG. 20.— Our cluster fiducials mapped to the $[(V-K_S)_0, M_V]$ - and $[(V-J)_0, M_V]$ -planes using the reddenings and distance moduli given in Table 2. From left to right, corresponding to increasing metallicity, are M15 (solid black), M92 (dotted black), M13 (grey short-dashed), NGC 1851 (black long-dashed), M5 (black solid line), M71 (black dot-dashed) and NGC 6791 (grey long-short dashed).

fact, the RGB segments of the isochrones become systematically redder than the observed RGBs with decreasing $[\text{Fe}/\text{H}]$. It seems unlikely that errors in the model T_{eff} scale are sufficient to cause this problem, because the discrepancies are primarily on the $V-J$ and $V-K_S$ colour planes. The same MARCS-transformed isochrones are able to reproduce the CMDs of M92 derived from $BV(RI)_C$ photometry quite well. This seems to suggest that there are problems with the predicted J and K_S magnitudes at low metallicities, but we are not able to provide an explanation for the origin of such difficulties.

This work has been supported by the Natural Sciences and Engineering Research Council of Canada through a Discovery Grant to DAV. We are grateful to the anonymous referee for valuable comments. Additionally, CMB thanks Loic Albert and Aaron Dotter for insightful discussions which improved both the observations and analysis in this paper.

REFERENCES

- Alonso, A., Arribas, S., & Martínez-Roger, C. 1996, *A&A*, 313, 873
Alonso, A., Arribas, S., & Martínez-Roger, C. 1998, *A&A*, 139, 335
Alonso, A., Arribas, S., & Martínez-Roger, C. 1999, *A&A*, 140, 261
Anthony-Twarog, B. J., Twarog, B. A., & Mayer, L. 2007, *AJ*, 133, 1585
Belokurov, V. et al. 2006, *ApJ*, 647, L111
Belokurov, V. et al. 2007, *ApJ*, 654, 897
Belokurov, V. et al. 2007, *ApJ*, 658, 337
Bergbusch, P. A. & Vandenberg, D. A. 2001, *ApJ*, 556, 322
Boesgaard, A.M., King, J.R., Cody, A.M., Stephens, A., & Deliyannis, C. P. 2005, *ApJ*, 629, 832
Boesgaard, A.M., Jensen, E.E.C., & Deliyannis, C.P. 2009, *AJ*, 137, 4949
Brogaard, K., Bruntt, H., Grundahl, F., Clausen, J.V., Frandsen, S., Vandenberg, D.A., & Bedin, L.R. 2010, *A&A*, submitted
Bono G., Caputo F., Marconi M., 1995, *AJ*, 110, 2365
Cacciari, C., Caloi, V., Castellani, V., & Fusi Pecci, F., 1984, *A&A*, 139, 285C
Carraro, G., Villanova, S., Demarque, P., McSwain, M. V., Piotto, G., & Bedin, L. R. 2006, *ApJ*, 643, 1151
Carretta, E., & Gratton, R. G., 1997, *Astron. Astrophys. Suppl.*, 121, 95
Carretta, E., Bragaglia, A., Gratton, R. G., D’Orazi, V., & Lucatello, S. 2009, *A&A*, 508, 695
Carretta, E. et al. 2000, *ApJ*, 533, 215
Casagrande, L., Portinari, L., Flynn, C. 2006, *MNRAS*, 373, 13
Casagrande, L., Ramírez, I., Meléndez, J., Bessell, M., & Asplund, M. 2010, *A&A*, 508, 695
Cassisi S., Salaris M., Pietrinferni A., Piotto G., Milone A. P., Bedin L. R., Anderson J., 2008, *ApJ*, 672, L115
Cassisi, S., De Santis, R., & Piersimoni, A. M. 2001, *MNRAS*, 326, 342
Cassisi, S., Potekhin, A., Pietrinferni, A., Catalan, M., & Salaris, M. 2007, *ApJ*, 661, 1094
Cenarro, A., J., Peletier, R. F., Sanchez-Blazquez, P., et al. 2007, *MNRAS*, 374, 664
Chaboyer, B., Green, E. M., & Liebert, J. 1999, *AJ*, 117, 1360
Clem, J. L., Vandenberg, D. A., & Grundahl, F., Bell, R. A., 2004, *AJ*, 127, 1227
Clementini, G. Gratton, R. G., Carretta, E., & Seden, C. 1999, *MNRAS*, 302, 22
Cohen, J. C., & Sleeper, C. 1995, *AJ*, 109, 242
Collet, R., Asplund, M., & Trampedach, R., 2007, *A&A*, 469, 687
De Santis, R., & Cassisi, S. 1999, *MNRAS*, 308, 97
Durrell, P. R., & Harris, W. E. 1993, *AJ*, 105, 1420
Ferraro, F. R., Montegriffo, P. A., & Fusi-Pecci, F. 2000, *AJ*, 119, 1282
Ferraro, F., Valentini, E., & Origlia, L. 2006, *ApJ*, 649, 243
Friel, E. D. et al. 2002, *AJ*, 124, 2693
Frogel, J. A., Persson, S. E., Matthews, K., & Aaronson, M. 1978, *ApJ*, 220, 75
Frogel, J. A., Persson, S. E., & Cohen, J. G. 1981, *ApJ*, 246, 842
Frogel, J. A., Persson, S. E., & Cohen, J. G. 1983, *ApJ*, 53, 713
Gratton R.G., Carretta E., & Castelli F. 1996 *A&A*, 314, 191 (1996)
Grevesse, N., & Sauval, A. J. 1998, *Sp. Sci. Rev.*, 85, 161
Grocholski & Sarajedini. 2003, *MNRAS*, 345, 1015
Grundahl, F., Stetson, P. B., & Andersen, M. I. 2002, *A&A*, 395, 481
Grundahl, F., Vandenberg, D.A., & Andersen, M.I. 1998, *ApJ*, 500, 179
Gustafsson, B., Edvardsson, B., Eriksson, K., Jorgensen, U.G., Nordlund, A., & Plez, B., 2008, *A&A*, 486, 951
Harris W. E., 1996, *AJ*, 112, 1487
Hempel, M., Hilker, M., Kissler-Patig, M., Puzia, T. H., & Minniti, D. 2003, *A&A*, 405, 487

- Hodder P. J. C., Nemeč J. M., Richer H. B., Fahlman G. G. , 1992, *AJ*, 103, 460
- Holweger, H., & Müller, E. A. 1974, *Sol. Phys.*, 39, 19
- Jevremovic, D., Dotter, A., & Baron, E., 2007, *Publications of the Astronomical Observatory of Belgrade*, 82, 131
- Jørgensen, U. G., Jensen, P., Sørensen, G. O., & Aringer, B. 2001, *A&A*, 372, 249
- Kraft, R. P., & Ivans, I. I. 2003, *PASP*, 115, 143
- Kron G. E., Guetter H. H., 1976, *AJ*, 81, 817
- Kaluzny, J., & Rucinski, S. M. 1995, *A&AS*, 114, 1
- Kuchinski, L. E., Frogel, J. A., Terndrup, D. M., & Persson, S. E. 1995, *AJ*, 109, 1131
- Marta, M. et al. 2008, *Phys. Rev. C*, 78, 022802
- McCall, M.L. 2004, *AJ*, 128, 2144
- Meléndez, J., & Ramírez, I. 2004, *AJ*, 615, 2004
- Meléndez, J., & Ramírez, I. 2005, *ApJ*, 626, 465
- Michaud, G., Richard, O., Richer, J., & VandenBerg, D. A. 2004, *ApJ*, 606, 452
- Milone A. P. et al., 2008, *ApJ*, 673, 241
- Paltrinieri, B., Ferraro, F.R., Fusi Pecci, F., & Carretta, E. 1998, *MNRAS*, 293, 434
- Pinsonneault et al. 2004, *ApJ*, 600, 946
- Pont, F., Mayor, M., Turon, C., & VandenBerg, D. A. 1998, *A&A*, 329, 87
- Proffitt, C. R., & Michaud, G. 1991, *ApJ*, 371, 584
- Ramírez, I. & Meléndez, J. 2005, *ApJ*, 626, 446
- Ramírez, I. & Meléndez, J. 2005, *ApJ*, 626, 465
- Randich, S., Sestito, P., Primas, F., Pallavicini, R., & Pasquini, L. 2006, *A&A*, 450, 557
- Rejkuba, M. 2004, *A&A*, 413, 903
- Renzini, A. 2008, *MNRAS*, 391, 354
- Sandage, A. R., Lubin, L. M. and VandenBerg, D.A., 2003, *PASP*, 115, 1187
- Schlegel, D.J., Finkbeiner, D.P., and Davis, M. 1998, *ApJ*, 500, 525
- Skrutskie, M.F., Cutri, R. M., Stiening, R., et al. 2006. *AJ*, 131, 1163
- Smith, V. V., Lambert, D. L., & Nissen, P. E. 1998, *ApJ*, 506, 405
- Snedden, C., Kraft, R. P., Prosser, C. F., & Langer, G.E., 1991, *AJ*, 102, 2001
- Stetson, P. B. 1987, *PASP*, 99, 191
- Stetson, P. B. & Harris, W. E. 1988, *AJ*, 96, 909
- Stetson, P. B. 2000, *PASP*, 112, 925
- Stetson, P. B. 2005, *PASP*, 117, 563
- Stetson, P. B. 2009, in *The Ages of Stars*, IAU Symp. 258, eds. E. E. Mamajek, D. R. Soderblom, & R. F. G. Wyse (Cambridge U. Press, Cambridge), p. 197
- Tautvaišienė, G., Edvardsson, E., Tuominen, I., & Ilyin, L. 2000, *A&A*, 360, 495
- Taylor, B. J. 2007, *AJ*, 133, 370
- Twarog, B. A., Ashman, K. M., & Anthony-Twarog, B. J. 1997, *AJ*, 114, 2556
- Valenti, E., Ferraro, F., & Origlia, L. 2007, *AJ*, 133, 1287
- VandenBerg D. A., 2000, *ApJS*, 129, 315
- VandenBerg, D. A., Swenson, F. J., Rogers, F. J., Iglesias, C. A., & Alexander, D. R. 2000, *ApJ*, 532, 430
- VandenBerg, D. A., Richard, O., Michaud, G., & Richer, J. 2002, *ApJ*, 571, 487
- VandenBerg, D. A., & Poll, H. E. 1989, *AJ*, 98, 1451
- VandenBerg, D.A., Clem, J. L., 2003, *AJ*, 126, 778
- VandenBerg D. A., 2005, *ASP Conference Series*, eds. D. Valls-Gabaud & M. Chavez, 2006, in press
- VandenBerg D. A., 2008, *Physica Scripta*, 133, 14026
- VandenBerg, D. A., Bergbusch, P. A., & Dowler, P. D. 2006, *ApJS*, 162, 375
- VandenBerg, D. A., Edvardsson, B., Eriksson, K., & Gustafsson, B. 2008, *ApJ*, 675, 746
- VandenBerg, D. A., Casagrande, L., & Stetson, P. B. 2010, *AJ*, submitted (VCS10)
- van Leeuwen, F. 2007, *A&A*, 474, 653
- Weiss, A. 2008, *Physica Scripta* T133, 014025
- Zinn, R., & West, M. J., 1984, *AJS*, 55, 45

V	$V-J$	V	$V-J$
19.817	2.062	17.411	1.762
19.659	2.001	17.437	1.831
19.515	1.944	17.476	1.897
19.363	1.889	17.485	1.953
19.215	1.840	17.459	2.011
19.067	1.787	17.376	2.043
18.924	1.738	17.263	2.058
18.771	1.692	17.109	2.071
18.633	1.656	16.959	2.091
18.486	1.625	16.809	2.114
18.331	1.595	16.659	2.130
18.172	1.567	16.509	2.152
18.011	1.548	16.359	2.164
17.845	1.529	16.209	2.186
17.676	1.528	16.059	2.211
17.516	1.548	15.909	2.236
17.388	1.588	15.759	2.264
17.357	1.639	15.609	2.299
17.367	1.699		

TABLE 3
FIDUCIAL SEQUENCE FOR THE OPEN CLUSTER NGC 6791 AS SHOWN IN FIGURE 2.

V	$V-J$	$V-K_S$	V	$V-J$	$V-K_S$
19.505	1.805	2.408	15.854	2.080	2.734
19.338	1.757	2.338	15.627	2.120	2.766
19.168	1.712	2.273	15.426	2.152	2.798
18.991	1.670	2.214	15.217	2.177	2.835
18.807	1.635	2.163	14.986	2.209	2.880
18.622	1.604	2.138	14.736	2.247	2.935
18.429	1.576	2.099	14.538	2.274	2.974
18.232	1.555	2.068	14.356	2.306	3.020
18.029	1.542	2.051	14.177	2.342	3.071
17.824	1.542	2.040	13.993	2.381	3.129
17.634	1.563	2.110	13.818	2.422	3.187
17.500	1.611	2.199	13.646	2.465	3.250
17.445	1.673	2.278	13.459	2.516	3.324
17.439	1.745	2.353	13.305	2.562	3.390
17.441	1.814	2.424	13.139	2.648	3.481
17.396	1.882	2.492	12.906	2.733*	3.619*
17.267	1.931	2.564	12.693	2.833*	3.800*
17.084	1.959	2.606	12.523	2.962*	3.970*
16.885	1.977	2.631	12.347	3.137*	4.164*
16.688	1.989	2.649	12.212	3.300*	4.350*
16.485	2.021	2.667	12.116	3.469*	4.552*
16.268	2.035	2.687	12.035	3.717*	4.883*
16.060	2.070	2.709	11.997	4.109*	5.401*

TABLE 4
FIDUCIAL SEQUENCES FOR THE GLOBULAR CLUSTER M71 AS SHOWN IN FIGURE 3. DUE TO THE SPARSENESS OF THE RGB, THOSE POINTS WITH $V < 13$ ARE MARKED BY ASTERISKS TO INDICATE THEY HAVE LARGE UNCERTAINTIES ASSOCIATED WITH THEM.

V	$(V-J)$	V	$(V-J)$
21.95	2.01	17.74	1.42
21.84	1.96	17.54	1.46
21.60	1.84	17.32	1.47
21.37	1.74	17.08	1.48
21.16	1.65	16.83	1.50
20.95	1.56	16.57	1.51
20.75	1.50	16.33	1.54
20.55	1.43	16.05	1.57
20.36	1.36	15.81	1.60
20.16	1.30	15.55	1.63
19.96	1.26	15.27	1.67
19.75	1.21	15.04	1.70
19.53	1.17	14.80	1.74
19.31	1.12	14.57	1.79
19.07	1.08	14.35	1.84
18.83	1.05	14.14	1.89
18.59	1.03	13.91	1.95
18.34	1.05	13.71	2.00
18.14	1.09	13.49	2.06
18.00	1.15	13.29	2.12
17.92	1.25	13.09	2.18
17.89	1.28	12.86	2.27
17.87	1.33	12.68	2.36
17.84	1.37	12.50	2.47
17.80	1.39	12.31	2.59

TABLE 5

FIDUCIAL SEQUENCE FOR THE GLOBULAR CLUSTER M 5 AS SHOWN IN FIGURE 5.

V	$V-K_S$	V	$V-K_S$
21.993	2.087	18.806	1.914
21.856	2.020	18.695	1.963
21.729	1.959	18.557	1.998
21.609	1.904	18.401	2.024
21.473	1.844	18.245	2.064
21.344	1.789	18.083	2.081
21.212	1.741	17.917	2.099
21.077	1.696	17.740	2.117
20.938	1.652	17.570	2.136
20.797	1.611	17.410	2.155
20.655	1.573	17.237	2.177
20.510	1.536	17.050	2.202
20.360	1.502	16.885	2.237
20.212	1.472	16.720	2.262
20.052	1.444	16.540	2.292
19.893	1.419	16.342	2.348
19.731	1.402	16.180	2.389
19.564	1.393	16.027	2.420
19.399	1.400	15.857	2.475
19.159	1.457	15.702	2.519
19.063	1.511	15.558	2.568
18.996	1.575	15.403	2.617
18.952	1.644	15.262	2.665
18.923	1.725	15.113	2.708
18.906	1.797	14.964	2.768
18.876	1.868	14.815	2.818

TABLE 6

FIDUCIAL SEQUENCE FOR THE GLOBULAR CLUSTER NGC 1851 AS SHOWN IN FIGURE 4.

V	$V-J$	$V-K_S$	V	$V-J$	$V-K_S$
22.039	2.011	2.606	17.548	1.331*	1.782*
21.884	1.939	2.513	17.420	1.360*	1.814*
21.740	1.883	2.416	17.271	1.381*	1.844*
21.606	1.832	2.344	17.112	1.397	1.868
21.460	1.766	2.267	16.952	1.411	1.888
21.306	1.709	2.176	16.786	1.424	1.907
21.173	1.653	2.120	16.433	1.451	1.945
21.030	1.596	2.042	16.104	1.478	1.974
20.891	1.541	1.988	15.747	1.511	2.031
20.761	1.501	1.931	15.585	1.527	2.050
20.640	1.455	1.868	15.408	1.546	2.072
20.502	1.414	1.801	15.214	1.569	2.104
20.372	1.368	1.760	15.036	1.601	2.145
20.249	1.334	1.712	14.880	1.620	2.173
20.112	1.299	1.662	14.715	1.643	2.215
19.979	1.260	1.620	14.546	1.667	2.249
19.839	1.220	1.578	14.393	1.697	2.298
19.700	1.182	1.518	14.238	1.722	2.342
19.560	1.146	1.491	14.088	1.748	2.379
19.411	1.119	1.454	13.945	1.774	2.415
19.263	1.095	1.419	13.800	1.802	2.475
19.113	1.063	1.397	13.646	1.843	2.529
18.962	1.042	1.369	13.499	1.875	2.573
18.800	1.024	1.342	13.360	1.907	2.628
18.637	1.008	1.320	13.211	1.944	2.689
18.472	0.999	1.327	13.051	1.999	2.768
18.306	0.999	1.338	12.923	2.053	2.818
18.152	1.014	1.368	12.787	2.104	2.880
18.022	1.043	1.430	12.642	2.182	2.952
17.923	1.083*	1.506*	12.487	2.258	3.058
17.842	1.139*	1.556*	12.289	2.373	3.223
17.751	1.192*	1.632*	12.152	2.474	3.352
17.692	1.242*	1.684*	12.005	2.612	3.547
17.642	1.290*	1.734*	11.895	2.729	3.741

TABLE 7

FIDUCIAL SEQUENCES FOR THE GLOBULAR CLUSTER M 13 AS SHOWN IN FIGURE 6. DUE TO THE LACK OF SUFFICIENT DATA AT SOME MAGNITUDES, ISOCHRONES WERE USED TO DETERMINE THE FIDUCIAL POINTS INDICATED BY ASTERISKS. THEREFORE THESE POINTS HAVE LARGE UNCERTAINTIES ASSOCIATED WITH THEM.

V	$V-J$	$V-K_S$	V	$V-J$	$V-K_S$
21.994	1.833	2.309	17.541	1.326*	1.758*
21.836	1.752	2.241	17.418	1.346*	1.800*
21.688	1.684	2.177	17.279	1.368*	1.832*
21.550	1.621	2.119	17.130	1.376*	1.857*
21.420	1.570	2.064	16.970	1.391*	1.880*
21.187	1.474	1.969	16.801	1.406*	1.901*
21.064	1.433	1.920	16.623	1.421*	1.922*
20.924	1.384	1.867	16.453	1.435*	1.942*
20.792	1.347	1.818	16.292	1.448	1.961
20.667	1.314	1.772	16.118	1.463	1.982
20.537	1.280	1.725	15.929	1.479	2.005
20.403	1.247	1.678	15.637	1.507	2.054
20.273	1.216	1.635	15.456	1.525	2.080
20.142	1.186	1.593	15.256	1.547	2.109
20.000	1.155	1.549	15.089	1.565	2.136
19.859	1.127	1.509	14.925	1.595	2.162
19.716	1.099	1.470	14.744	1.627	2.201
19.572	1.073	1.432	14.541	1.653	2.247
19.422	1.047	1.396	14.321	1.692	2.308
19.267	1.023	1.361	14.140	1.727	2.357
19.105	1.000	1.328	13.984	1.761	2.399
18.938	0.980	1.300	13.827	1.783	2.433
18.780	0.965	1.278	13.682	1.818	2.467
18.617	0.953	1.261	13.528	1.857	2.505
18.451	0.951	1.259	13.379	1.889	2.544
18.294	0.963	1.276	13.236	1.920	2.583
18.164	0.990*	1.314*	13.085	1.964	2.626
18.062	1.026*	1.365*	12.933	1.999	2.675
17.981	1.068*	1.415*	12.798	2.046	2.730
17.912	1.113*	1.450*	12.655	2.086	2.787
17.852	1.163*	1.521*	12.503	2.147	2.854
17.803	1.210*	1.589*	12.362	2.208	2.922
17.751	1.261*	1.662*	12.235	2.262	2.998
17.652	1.300*	1.723*	12.103	2.332	3.108

TABLE 8

FIDUCIAL SEQUENCES FOR THE GLOBULAR CLUSTER M92 AS SHOWN IN FIGURE 8. DUE TO THE LACK OF SUFFICIENT DATA AT SOME MAGNITUDES, ISOCHRONES WERE USED TO DETERMINE THE FIDUCIAL POINTS INDICATED BY ASTERISKS. THEREFORE THESE POINTS HAVE LARGE UNCERTAINTIES ASSOCIATED WITH THEM.

V	$V-J$	$V-K_S$	V	$V-J$	$V-K_S$
22.010	1.764	2.140	17.979	1.468*	1.932*
21.887	1.694	2.079	17.830	1.476*	1.957*
21.764	1.653	2.030	17.670	1.491*	1.980*
21.624	1.604	1.977	17.501	1.506*	2.001*
21.492	1.547	1.928	17.323	1.521	2.022
21.367	1.504	1.882	17.153	1.535	2.072
21.237	1.450	1.835	16.992	1.548	2.081
21.103	1.417	1.788	16.818	1.563	2.122
20.973	1.366	1.745	16.629	1.579	2.145
20.842	1.326	1.703	16.337	1.607	2.204
20.700	1.277	1.659	16.156	1.625	2.230
20.559	1.247	1.619	15.956	1.647	2.259
20.416	1.199	1.580	15.789	1.665	2.296
20.272	1.173	1.542	15.625	1.695	2.302
20.122	1.147	1.506	15.444	1.727	2.331
19.967	1.123	1.471	15.241	1.753	2.367
19.805	1.100	1.438	15.021	1.792	2.418
19.638	1.080	1.410	14.840	1.827	2.457
19.480	1.065	1.388	14.684	1.861	2.499
19.317	1.053	1.371	14.527	1.883	2.523
19.151	1.051	1.369	14.382	1.918	2.557
18.994	1.063	1.386	14.228	1.957	2.595
18.864	1.090	1.424	14.079	1.989	2.644
18.762	1.126	1.475	13.936	2.020	2.683
18.681	1.168*	1.535	13.785	2.064	2.726
18.612	1.213*	1.600	13.633	2.099	2.785
18.552	1.263*	1.671	13.498	2.146	2.850
18.503	1.310*	1.739	13.355	2.186	2.907
18.451	1.361*	1.772	13.203	2.227	2.976
18.352	1.400*	1.833	13.062	2.278	3.062
18.241	1.426*	1.858*	12.935	2.322	3.128
18.118	1.446*	1.900*	12.803	2.382	3.208

TABLE 9

FIDUCIAL SEQUENCES FOR THE GLOBULAR CLUSTER M 15 AS SHOWN IN FIGURE 7. DUE TO THE LACK OF SUFFICIENT DATA AT SOME MAGNITUDES, ISOCHRONES WERE USED TO DETERMINE THE FIDUCIAL POINTS INDICATED BY ASTERISKS. THEREFORE THESE POINTS HAVE LARGE UNCERTAINTIES ASSOCIATED WITH THEM.